Raman spectroscopy determination of phases within thermal sprayed hydroxyapatite splats and subsequent in vitro dissolution examination

H. Li [a], B.S. Ng [a], K.A. Khor [a,*], P. Cheang [b], T.W. Clyne [c]

[a] *School of Mechanical and Production Engineering, Nanyang Technological University, 50 Nanyang Avenue, Singapore 639798, Singapore*
[b] *School of Materials Engineering, Nanyang Technological University, 50 Nanyang Avenue, Singapore 639798, Singapore*
[c] *Department of Materials Science and Metallurgy, University of Cambridge, CB2 3QZ, UK*

Abstract

Phase compositions at various locations within individual thermal sprayed hydroxyapatite (HA) splats were qualitatively determined using Raman spectroscopy analysis and, confirmed through in vitro dissolution exercise. The purpose of the present study was to verify the locations of different phases within a HA splat deposited by thermal spray techniques. The splats were prepared through dc thermal plasma and high velocity oxy-fuel (HVOF) spray processes. Raman spectroscopy studies were performed to determine the locations of various phases that exist within individual splats, and the results were verified with in vitro dissolution tests. Results showed that the Raman spectroscopy is a feasible technique for qualitative determination of the phases within a single HA splat. It was revealed that the thermal decomposition of HA into tricalcium phosphate (TCP), amorphous calcium phosphate (ACP), tetracalcium phosphate (TTCP), CaO and other phases, occurred mainly within the melted portion of the sprayed particle during the thermal spray process. The in vitro tests of the individual HA splats in simulated body fluid established a reasonable correlation between localized dissolution behavior and the phases revealed by the Raman spectroscopy plots. This study demonstrates the feasibility of employing the Raman spectroscopy technique to provide phase distribution information within a single HA splat. Henceforth, a better understanding and control of optimizing the properties of a bulk HA coating through controlling the spray process could be possible.
© 2003 Acta Materialia Inc. Published by Elsevier Ltd. All rights reserved.

Keywords: Raman spectroscopy; Plasma spray; High velocity oxy-fuel; Hydroxyapatite; Splat; In vitro

1. Introduction

Hydroxyapatite (HA) coatings deposited using thermal spray techniques on titanium alloy substrates showed propensity of avoiding the inherent mechanical property limitations of HA without significant loss in biocompatibility [1,2]. In order to elucidate the potential of HA in clinical applications, extensive investigations on the HA coatings have been conducted through in vitro and in vivo tests [3–5]. It was found that the macro- and microstructure of HA was extremely important for the apposition of bone [6]. The biological performances of the calcium phosphate (CP) coatings were actually phase-dependent and the biological behavior of the phases in HA family had been clarified [7,8]. It is therefore believed that optimization of the phase composition of as-sprayed CP coatings is a prerequisite towards establishing competitive properties for biomedical applications. Minimal transformation of HA during coating deposition is preferred. However, since the thermal spray is a high temperature process, the HA transformation is inevitable during coating preparation. It should be noted that the extent of thermal transformation of HA to α,β-tricalcium phosphates (TCP), tetracalcium phosphate (TTCP), or amorphous calcium phosphate (ACP) is closely related to the extent of melting of HA particles during coating deposition

* Corresponding author. Tel.: +65-6-790-5526; fax: +65-6-791-1859.
  E-mail address: mkakhor@ntu.edu.sg (K.A. Khor).

[9–11]. It is essentially important to study the distribution of the various calcium phosphates phases within the coating in order to achieve a better understanding, and hence, possible controlling of the biological performances of the coatings used as implants.

Furthermore, it is well known that a thermal sprayed coating shows a layered structure, which has an accumulated character composed of individual splats. Researchers have extensively concentrated on the study of thermal sprayed splats [12–14]. Generally, in most cases, as the substrate temperature is low (e.g., <500 °C), splat formation is an isolated progression, which infers that subsequent on-coming splats have minor influence on the phases of prior deposited splats. Therefore, the overall in vitro behavior of a bulk HA coating can arguably be intimately related to that of individual HA splats. A good understanding of the in vitro behavior of a single HA splat would significantly contribute to the knowledge on dissolution/precipitation mechanism of HA coatings. Therefore, a study on splats is essentially crucial towards establishing an understanding of individual splats' contribution to the phase composition of the thermal sprayed coating; and satisfactory control of phase composition of the coating through elucidation of phases' response within a splat. However, comprehension of phase composition within a single thermal sprayed splat is still inadequate due mainly to limitations faced with existing techniques.

In order to characterize the CP phases, which only differentiate slightly in structures, within a splat, a structure-sensitive and localized technique is required. Conventionally available techniques have their limitations; X-ray diffraction can only detect phases within a large area (in accordance to the classical Bragg–Brentano geometry), and do not provide sufficient information when amorphous phases are the major components. On the other hand, infrared spectrometry (IR) gives detailed information about molecular vibrations, however there is a lack in information of wavelength shift lower than 400 cm^{-1}. Infrared (IR) method cannot be utilized in phase determination within a thermal sprayed splat owing to the infeasibility of sample preparation. Raman spectroscopy technique, on the other hand, could provide information on the short- and intermediate-range ordering in the solids. It allows a direct and nondestructive detection from the sample surface with spatial resolution (micrometric) 100 times higher than the infrared resolution. Since the biological performances of the CP deposits, both in vitro and in vivo, are significantly dependent on their phases [7,8], and the local phases do play an extremely important role in determining their behaviors [15], the study on the detailed structure information using the Raman spectroscopy technique could be essentially important. However, to date, there is still inadequate knowledge in understanding the phase changes within minor zones (<50 µm) of HA splats. The present study aims to use the

Raman spectroscopy to qualitatively determine the phases within individual thermal sprayed CP splats. In order to further understand the feasibility of the use of Raman technique, in vitro dissolution was also conducted through incubating the splats in simulated body fluid (SBF) over different durations. In the present study, plasma sprayed and high velocity oxy-fuel (HVOF) sprayed HA splats were collected, and investigated for structural characterization and in vitro dissolution evaluation in SBF.

2. Experimental materials and setup

In-house synthesized HA powders [16] were utilized for the splats deposition employing both HVOF and plasma spray processes. These powders were heat-treated at 800 °C for 5 h and XRD detections were performed to ensure their major component is stoichiometric HA. The HA powders with two different particle size ranges, 25–45 µm and 45–75 µm, were investigated. The particle size distribution of the starting powders used in the present study was analyzed using a laser particle size analyzer (Analysette 22, Fritsch Gmbh, Germany). Two sets of data, quantity percentage of individual particles in terms of size in diameter and the distribution density of the particles, were determined. Figs. 1(a) and (b) show the particle size distribution curves and topographical morphology of the typical starting HA powders Fig. 1(c). A fully computerized HV2000 HVOF system (Praxair Thermal Spray Inc, IN, USA) with a 19 mm nozzle, and SG100 plasma system (Praxair Thermal Spray Inc, IN) were utilized for the splats preparation. The nozzle diameter of the SG100 plasma torch used is 7.96 mm. The diameter of the powder injector is 1.74 mm and the location of the injector is within the nozzle near the gun exit (internal injection). The spray parameters of HVOF spraying and plasma spraying are tabulated in Table 1. The HA splats were collected on polished Ti–6Al–4V plate substrates. The powders with a wide range of sizes were sprayed to prepare splats with different morphology on the polished substrates. A shielding plate was placed between the substrate and flame/arc to catch single HA splat and several holes of 1 mm in diameter were drilled on the plate. Fig. 2 schematically depicts the procedure setup for the HA splat collection. In the present study, the spray process was conducted for only one pass to acquire the individual splats. It was found that the substrate temperature during the spraying was lower than 100 °C.

During the in vitro testing, the splats samples were incubated in the SBF solution for various durations to reveal their dissolution behavior. The substrate on which the HA splats were deposited used for in vitro tests was of the dimension of $12 \times 12 \times 2$ mm^3 in width,
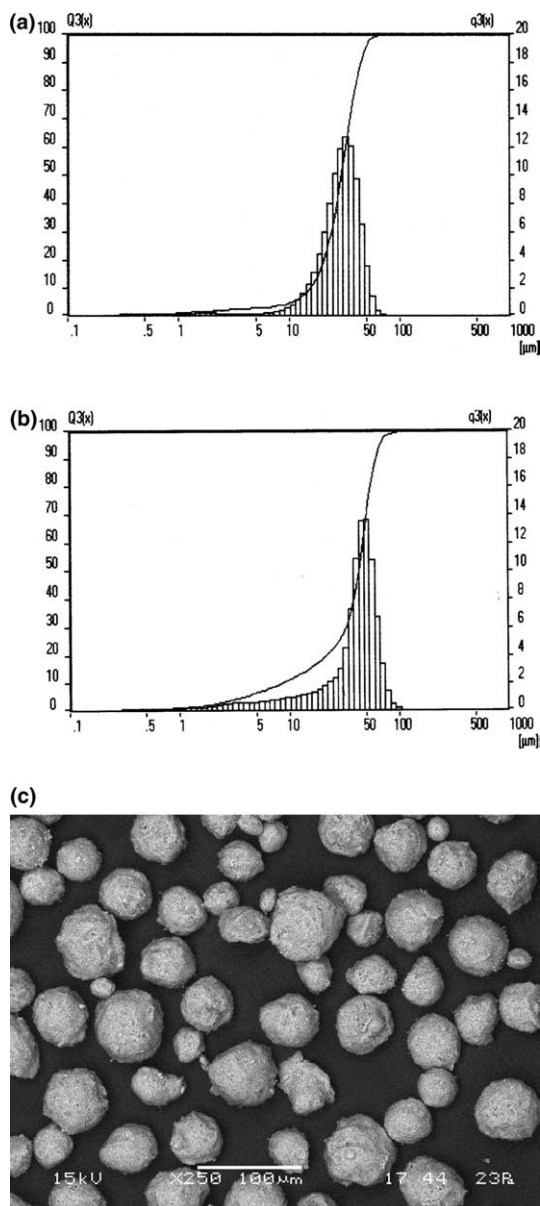
Fig. 1. Particle size distribution, (a) 25–45 μm, (b) 45–75 μm, and the topographical morphology (c) of the starting HA powders.

Table 1
Spray parameters for the HA splats preparation

Plasma spray	HVOF
Model: SG-100, Praxair, USA	Model: HV2000, Praxair, USA
Net energy: 12 kW	O^2: 283 L/min
Ar: 30.6 L/min	H^2: 566 L/min
He: 22.6 L/min	Carrier gas (Ar): 19 L/min
Carrier gas (Ar): 10 L/min	Powder feed rate: 8 g/min
Powder feed rate: 10 g/min	Spray distance: 250 mm
Spray distance: 120 mm	

length and width, respectively. The Kokubo SBF (pH 7.40) [17] was used for the in vitro incubation. The solution is composed of 142.0 mM Na^+, 5.0 mM K^+, 1.5
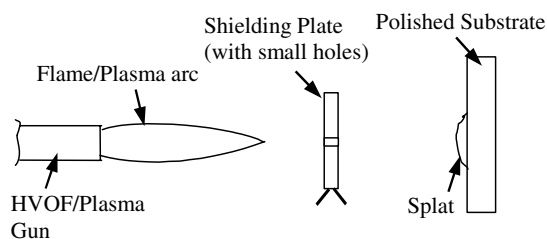

Fig. 2. Depiction of the experimental setup for individual HA splats collection.

mM Mg^{2+}, 2.5 mM Ca^{2+}, 147.8 mM Cl^-, 4.2 mM HCO_3^-, 1.0 mM HPO_4^{2-}, and 0.5 mM SO_4^{2-}. The in vitro test was conducted in a continuously stirred bath containing distilled water with a stable temperature of 37 °C. Each sample was incubated in 70 ml SBF contained in a polyethylene bottle. Once the sample was taken out from the solution, it was washed in distilled water and subsequently dried at ambient temperature. According to a previous study [18], post-spray annealing treatment at 750 °C brought about full recrystallization in the coatings. In the present study, heat treatment at 750 °C was conducted for 30 min on plasma sprayed HA splats. Raman spectroscopy analysis and in vitro incubation were also conducted for the heat-treated splats. Topographical features of the splats were observed by scanning electron microscopy (SEM, JEOL JSM-5600LV). The ImagePro image analysis software was used for the quantitative determination of the dissolution rates after incubation of the splats in the SBF.

The Raman scattering experiments were performed using a Renishaw Raman Imaging Microscope WiRE spectroscopy equipped with 50 mW Class 3B helium-neon Laser ($\lambda = 632.816$ nm). The probing spot was about 4 μm in diameter under $1000\times$ magnification in an optical transmission light microscope (Leica DML). The spectrometer was calibrated by recording the spectrum from Si sample with characteristic peak at 520 cm^{-1}. Spectra collected from commercial HA, α- and β-TCP powders (Taihei Chemical In. Co. Pte, Japan), CaO, $CaCO_3$ and CaOH (Merck KGaA, Germany) were used as references. XRD was done (not shown in this paper) on all these powders prior to Raman spectrometry to re-confirm their content. Spectra were collected from near edge and center of various HVOF sprayed, as-plasma-sprayed and heat-treated plasma-sprayed splats.

3. Results and discussion

3.1. Morphology of splats

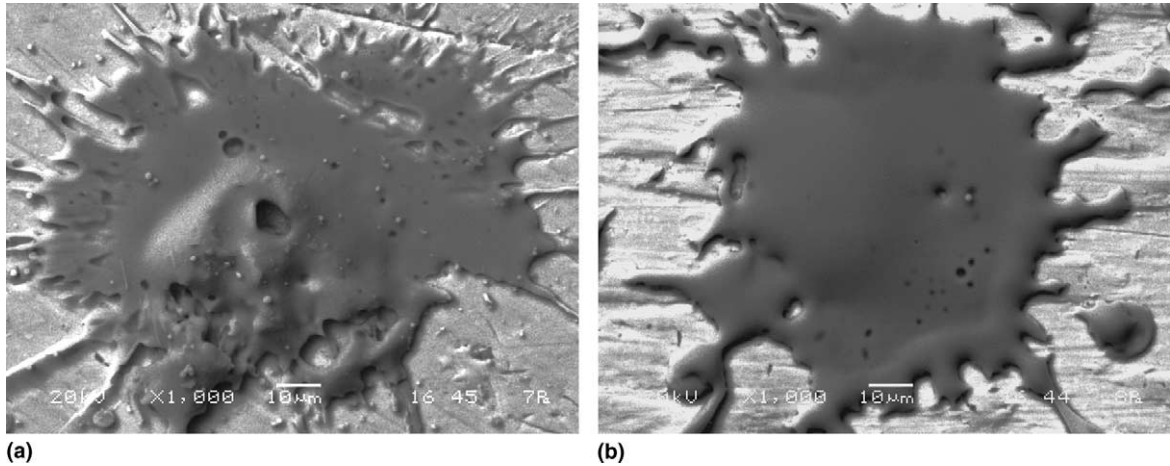The topographical microstructure of typical plasma and HVOF sprayed HA splats are shown in Fig. 3. The

Fig. 3. Typical topographical morphology of HVOF sprayed HA splat (a) and plasma sprayed HA splat (b). The substrate temperature is lower than 100 °C.

microstructure of the splats reveal a partial melt state of the HA particles during HVOF spray and a complete melt state of those during plasma spray.

3.2. Crystal structure

3.2.1. The 200–900 cm^{-1} region

The Raman spectra of the plasma sprayed HA splats (as-sprayed and heat-treated) are shown in Fig. 4. Fig. 5 shows the Raman spectra of a big and a small HVOF splat. The spectra of the reference materials are shown in Fig. 6.

3.2.2. The 900–2000 cm^{-1} region

The Raman spectra of the plasma sprayed HA splats (as-sprayed and heat-treated) are shown in Fig. 7. Fig. 8 shows the Raman spectra of a big and a small HVOF splat. The spectra of the reference materials are shown in Fig. 9.

Fig. 5. Raman shifts of a big HVOF splat at: (a) center, (b) edge and a small HVOF splat at (c) center and (d) edge.

Fig. 6. Raman shifts of the reference materials: (a) Ca(OH)$_2$, (b) CaCO$_3$, (c) CaO, (d) α-TCP and (e) β-TCP.

3.3. In vitro dissolution

Microstructure changes of the splats induced by the in vitro ageing are typically shown in Figs. 10 and 11.
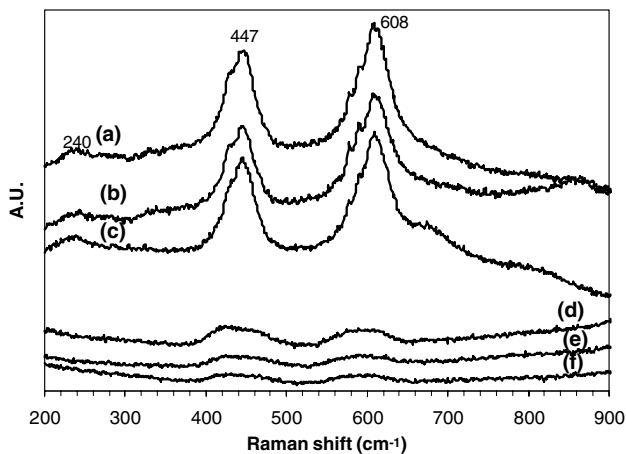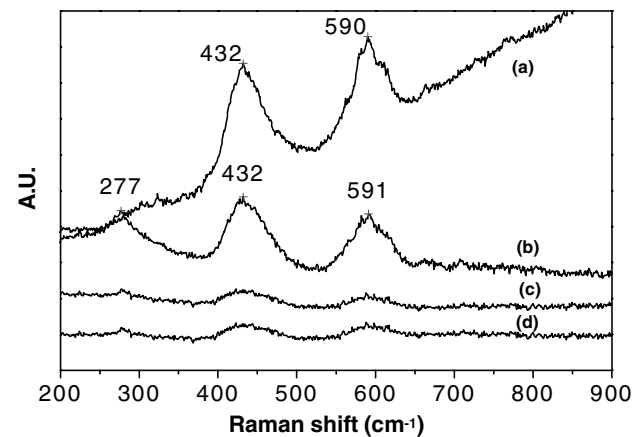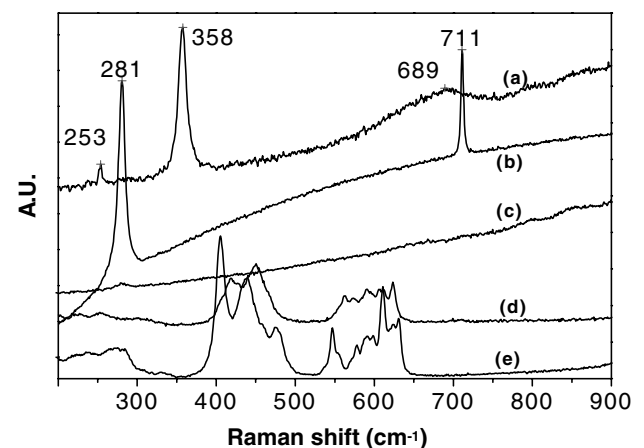

Fig. 4. Raman shifts of heat-treated HA splat (plasma sprayed) at: (a) middle, (b) edge and (c) center, and as-plasma-sprayed HA splat at (d) edge, (e) middle and (f) center of splat.
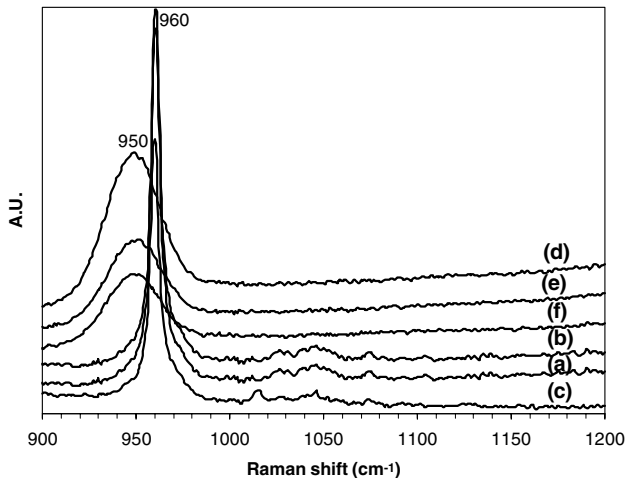
Fig. 7. Raman shifts of a typical heat-treated HA splat (plasma-sprayed) at: (a) middle, (b) edge and (c) center, and as-plasma-sprayed HA splat at (d) edge, (e) middle and (f) center.
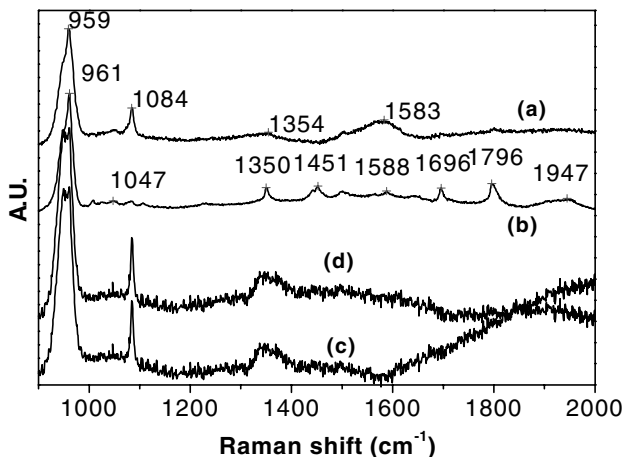

Fig. 8. Raman shifts of the big HVOF HA splat at: (a) edge, (b) center and the small HVOF HA splat at (c) edge and (d) center.
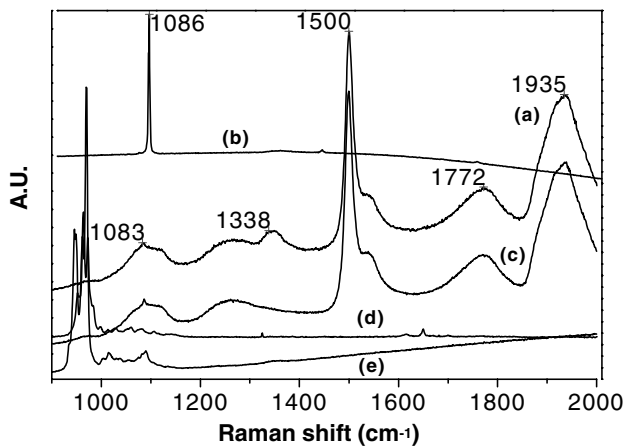

Fig. 9. Raman shifts of the reference materials: (a) Ca(OH)$_2$, (b) CaCO$_3$, (c) CaO, (d) α-TCP and (e) β-TCP (900–2000 cm^{-1}).

Additionally, effect of incubation duration on the histological changes is also demonstrated. The influence of post-spray crystallization treatment on the in vitro dissolution behavior of the splats was also investigated. Results showed that 3 days in vitro ageing has no obvious influence on the microstructure changes of the heat-treated HA splats. For these HA splats, no obvious dissolution can be claimed. Fig. 12 shows the dissolution rates (defined here as the ratio of dissolved area to overall area of a splat) of both the plasma sprayed and HVOF sprayed HA splats under the present spray parameters. It is noted that partially melted powders show a remarkably low dissolution rate.

4. Discussion

The difference in melt state of the powders during HVOF and plasma spray (Fig. 3) is likely due to the decidedly different temperatures of the heating sources, and consequently, the amount of heat input. Furthermore, the residence time of the particles in the heating source also contributes to their melt state. The surface temperatures of the HA particles during plasma spraying were measured using a CCD camera system (SprayWatch-2i, Oseir, Finland). According to the requirement of the SprayWatch system, the distance between the CCD camera and the HA particle flux was 250 mm. And the data obtained was an average value calculated from the detected particle flux within a volume of $34 \times 27 \times 25$ mm^3. The highest temperature attained by the HA powders during the plasma spraying is up to 2288 °C. However, unfortunately, the temperatures of in-flight HA particles within HVOF spraying cannot be measured owing to their far lower surface temperature, which is lower than the detectable values of the current CCD camera. It has been extensively reported that decomposition of HA started at the temperatures higher than 1000 °C, therefore, significant phase transformation from HA to other CP would take place during the plasma spraying due to the high temperatures attained by the powders, >2200 °C.

It is noted that for the plasma-sprayed HA splats, there is a lack of obvious Raman shifts at the miscellaneous locations as shown in Figs. 4(d)–(f) and Figs. 7(d)–(f). The broadening and featureless bands at vibration modes v_1 ($\sim$950 cm^{-1}), v_2 ($\sim$430 cm^{-1}), v_4 ($\sim$596 cm^{-1}), and the almost unobservable peaks of v_3 ($\sim$1032–1081 cm^{-1}) are typical features of ACP structure [19]. These indicate the presence of uniform ACP phase within the splat; a result of fully melted HA powders during the plasma-spray process. Upon heat treatment, the bands of the respective vibration modes were narrowed, with an increased intensity and splitting of peaks (v_2 – 428 and 447 cm^{-1}, v_3 – 1029, 1044, and 1075 cm^{-1}, and v_4 – 575, 589, and 608 cm^{-1}). The main v_1 peak is
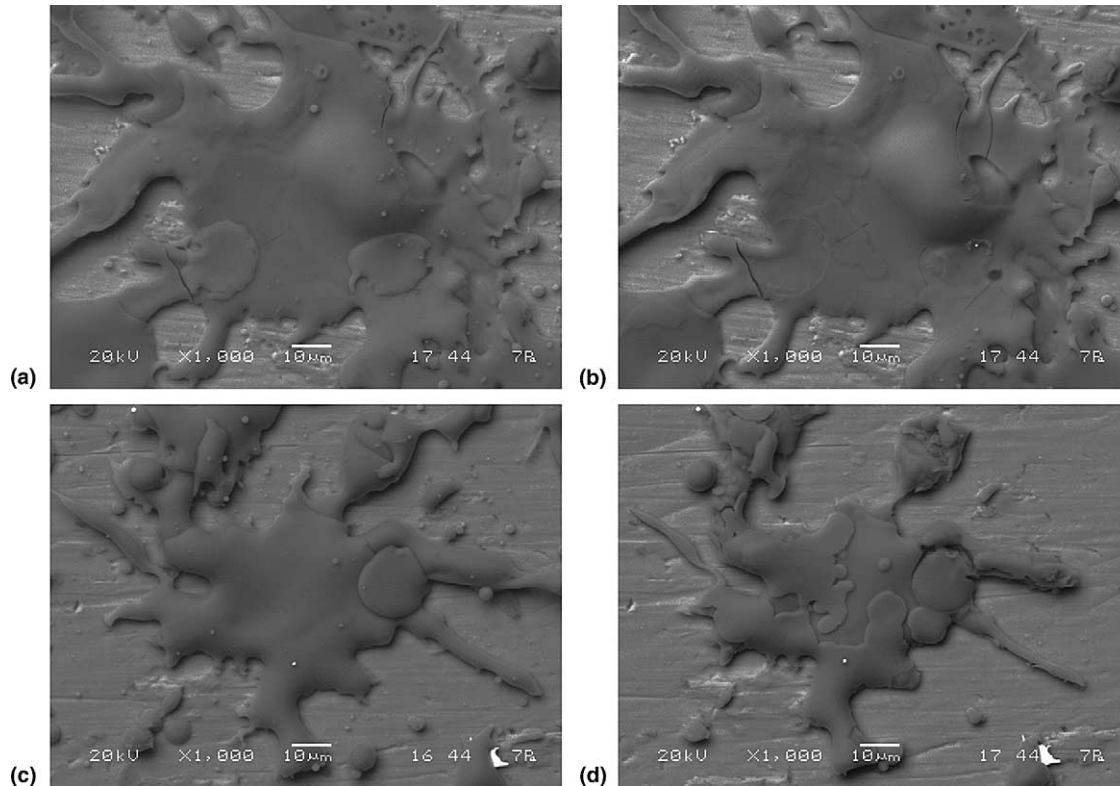
Fig. 10. Typical histological changes of plasma sprayed HA splats after 30 min (a-1 before, a-2 after) and 1 h (b-1 before, b-2 after) incubation showing obvious dissolution. The substrate temperature is lower than 100 °C. Magnification: ▬▬ 10 μm.

also observed to have narrowed and shifted from center of $\sim$950 to $\sim$960 cm^{-1}, which is assigned to a typical feature of crystalline HA [19–22]. The results from Raman technique tallies with the previous studies [18], as it was found that the heat treatment bought about full crystallization from ACP to HA. However, the presence of small shoulders at $\sim$952, 972, and 982 cm^{-1}, around v_1 mode peak indicates presence of small amount ($\sim$5%) of α-TCP.

For the small HVOF splats (made from small HA powders with a diameter <45 μm), it was observed that within the 200–900 cm^{-1} region, the bands for vibration modes v_2 and v_4 (Figs. 5(c) and (d)) are very similar to those of the as-plasma-sprayed splats. The main v_1 mode band, however, splits into 949, 952, and 961 cm^{-1} (Figs. 8(c) and (d)) and the base spread over a range from 927 to 977 cm^{-1}. When compared to the peaks of the reference materials shown in Figs. 9(d) and (e), these peaks corresponds with those of α-TCP (951, 963, 972, 982 cm^{-1}) and β-TCP (934, 946, 949, 962, 969 cm^{-1}). The spectra at $\sim$280, 1084, and 1354 cm^{-1} originated from the presence of CaCO$_3$. Again, no obvious difference in the Raman shifts is observed for spectra collected from the splat's edge and center. It is proposed that for small HVOF splats, HA powders were near fully melted and decomposed during deposition. There is a uniform distribution of ACP, α-TCP, β-TCP, CaCO$_3$ and very small amount of unmelted HA. The CaCO$_3$ is likely

originated from hydrolyzed CaO (decomposition product of HA), which formed Ca(OH)$_2$ and reacted with CO$_2$ in air.

Raman spectra for large HVOF splats (made from HA powders with a diameter >45 μm) have comparatively narrower spread at the various PO$_4^{3-}$ vibration modes (Figs. 5(a) and (b) and Figs. 8(a) and (b)). Within the 200–900 cm^{-1} regions, spectra of vibration modes v_2 ($\sim$432 cm^{-1}) and v_4 ($\sim$591 cm^{-1}) are of higher intensity with splitting of peaks observed as compared to those collected from small splats, a characteristic of higher degree of crystallinity [19]. And such splitting of peaks is more prominent on the spectra collected from center of the splat. The base of the bands from v_2 and v_4 modes stretched over a broader range with greater number of peak splitting than those from HA, suggesting the presence of α- and β-TCP [20]. The main v_1 bands for the edge and center of the splat are 959 and 962 cm^{-1}, respectively; typical peaks of HA [19,20]. The 2 cm^{-1} differences are insignificant as it is the same as the Raman spectrometer slit size [22]. The shoulder at the 944 cm^{-1} band strongly indicates the presence of α-TCP, while the spread of its base from 924 to 983 cm^{-1} bands suggested the presence of some amount of β-TCP. The lower intensity of the 1084 cm^{-1} band in spectra collected from the center of the splat is likely due to a lower CaCO$_3$ content. The splitting of peaks at v_3 (1004, 1024, 1047, and 1104 cm^{-1}) once again suggested the
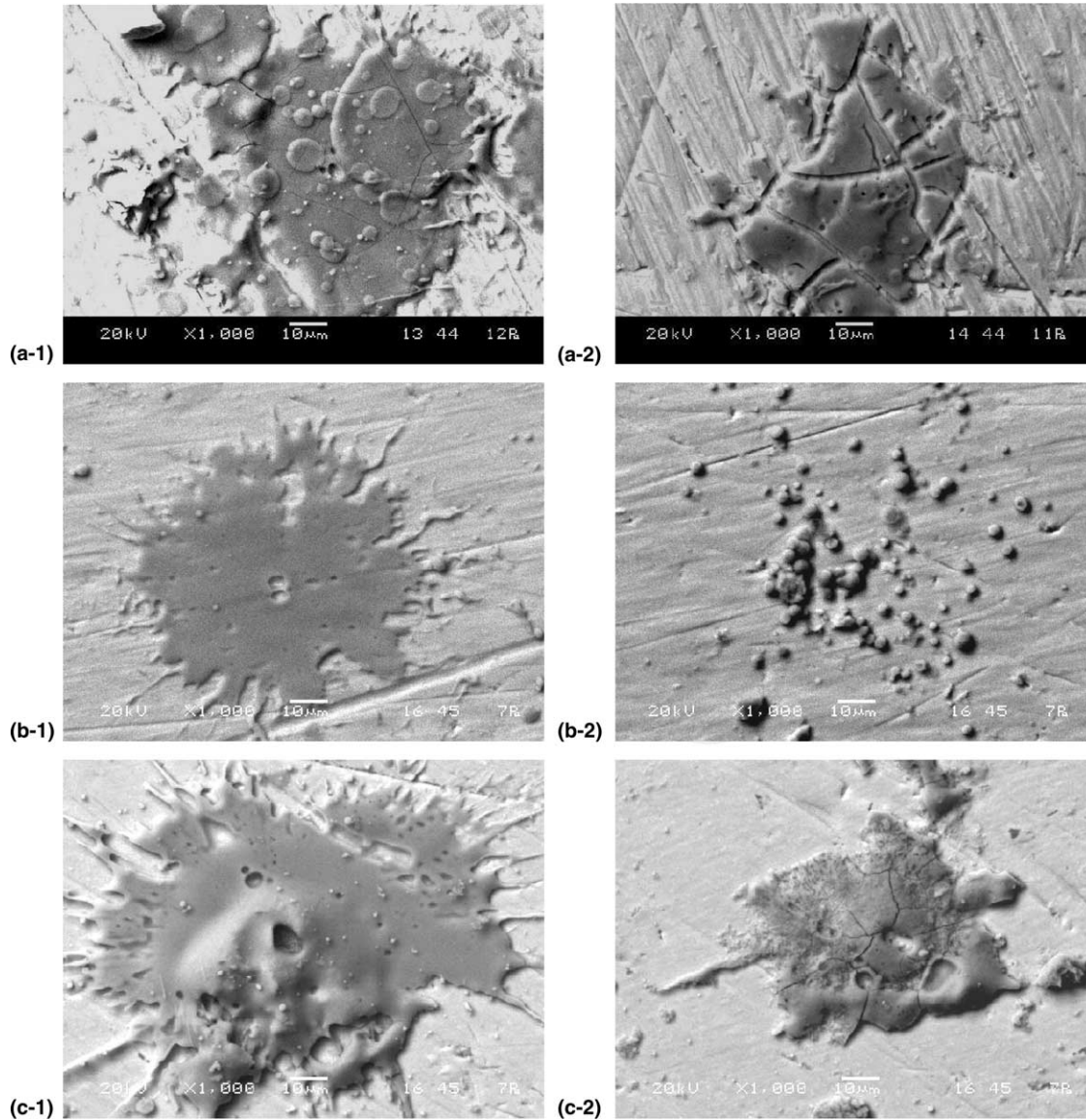
Fig. 11. Typical histological changes of HVOF sprayed HA splats after (a) 2 h and (b) 3 days in vitro incubation showing remarkable influence of incubation time and particle's melt state on the obvious dissolution (1 before incubation, 2 after incubation). The micrographs (b,c) have the same magnification as the micrographs (a). The substrate temperature is lower than 100 °C.

co-existence of HA, α- and β-TCP. Overall, the Raman spectra of HVOF splats suggested that the HA powders are only partially decomposed, which must be attributed to their partially melted state during deposition. Highest degree of crystallinity exist at the center of the big splat, with HA and α-TCP being the two main phases. The amount α-TCP and $CaCO_3$ increases from the center towards the edge of the splat together with a decrease in crystallinity. This could be a result of temperature gradient within the HA particle during the deposition. With the lowest temperature at the center, material around this region experienced lower degree of transformation and decomposition. Small HVOF HA splat has a uniform spread of phases, with higher content of α-TCP and $CaCO_3$ and overall lower crystallinity. The present

Raman results correspond very well with our previous findings on the influence of HA particle size on phase composition of resultant HVOF coating [16].

The in vitro dissolution rates (Fig. 12) together with the microstructural changes of the splats (Figs. 10 and 11) confirm the possible phases within different locations revealed by the Raman detection. It was revealed that surrounding part of the splats (Figs. 10 and 11) preferably dissolved into the SBF. It has been determined that the dissolution rate of different CP phases in the SBF is in the order HA < CDHA < OHA < β-TCP < α-TCP < TTCP < ACP [23]. The current dissolution results of the splats fit very well with their Raman spectra at different zones (Figs. 4–9). It is noted that even under full melt state of the sprayed HA powders, plasma spray
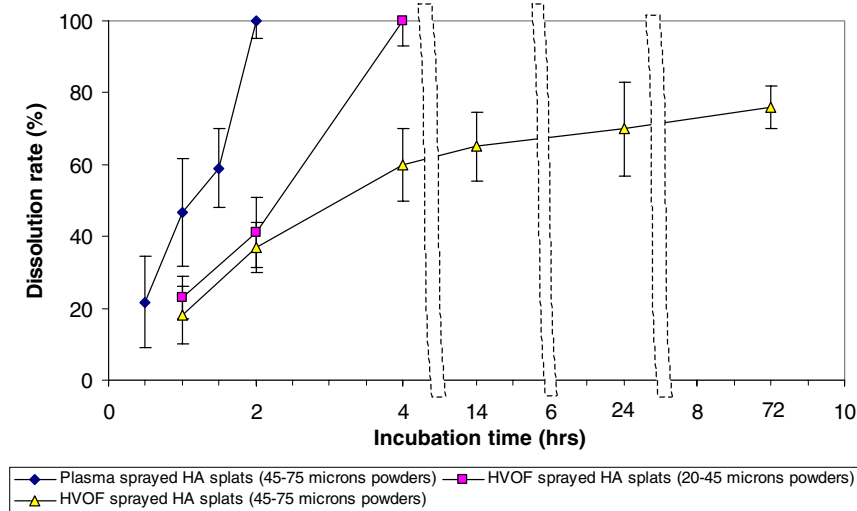
Fig. 12. In vitro dissolution rates of the HA splats prepared by plasma and HVOF spraying different HA powders, showing remarkable influence of spray processes and melt state of the powders on the dissolution rate of resultant splats.

(45–75 μm) and HVOF (20–45 μm) showed different effect on the dissolution behaviors of the splats (Fig. 12). The present results revealed that under the same full melt state, the dissolution rates of the resultant splats are different depending on the phases present within the splats. On the other hand, the obvious dissolution of the splats has indicated their remarkable biocompatibility. For the plasma sprayed HA splats, 2 h resulted in full dissolution of the phases while 4 h for HVOF sprayed HA splats (fully melted). For the partially melted HVOF splats, a precipitation appeared after 24 h of incubation, and the dissolution reached a proximately stable state after 14 h, which indicates extremely low dissolvability of crystalline HA. According to previous studies on phase transformations of HA at elevated temperatures [24,25], the present results further confirmed that HA decomposition mainly occurred within the melted part of the sprayed particles. In other words, there could be a relationship between melt states of HA particles during the spraying and phase composition of the resultant splat. A previous study [26] and other ancillary results on dissolution behaviors of various CP phases [27] have pointed out that, compared to crystalline HA, TCP, and TTCP, ACP preferably dissolved within SBF. It has also been found that for a structure with a complex phase composition, preferable dissolution still occurred, TCP preferably dissolved and it resulted in remarkable voids within a CP coating [27].

In a previous report [18], the decomposition of HA during the HVOF spraying was inevitable. The only difference between the splats deposited by HVOF spraying and plasma spraying is the extent to which the phase transformation occurs, that is, there is much less transformation during HVOF spraying than that in plasma spraying. It should be noted that the pres-

ent Raman analysis results revealed the main content of ACP within the plasma sprayed HA splats. Since the present study only studied the splats intimately adhering to the substrate, it is not surprising that more ACP can be resulted within the splats close to substrate surface than those far away from the substrate surface. Other researchers [19,28] have also experimentally confirmed the phenomenon.

5. Conclusions

The Raman spectroscopy analyses qualitatively revealed the phases within different zones of both the plasma sprayed and HVOF sprayed HA splats. In vitro dissolution tests of the splats confirmed the results detected by the Raman technique. Use of the Raman spectroscopy together with in vitro dissolution provides the possibility of determining phases within a thermal sprayed HA splat. The results showed that HA decomposition occurred mainly within the melted part of a thermal sprayed HA particle and the surrounding part of a splat is mainly responsible for the quick dissolution of the splats in vitro. The difference in phase composition of HA splats, and hence, the extent of HA transformation during thermal spraying, could be well explained by the remarkable differences in the particle temperatures and temperature gradient within a particle during the spraying.

References

[1] Oonishi H, Yamamoto M, Ishimau H, Tsuji E, Kushi-tani S, Aono M, Ukon Y. J Bone Joint Surg 1989;10:213.

[2] Hardy DCR, Frayssinet P, Delince PE. Eur J Orthop Surg Traumatol 1999;9:75.

[3] Wang BC, Chang E, Yang CY. Mater Chem Phys 1994;37:55.

[4] Tranquilli PL, Merolli A, Palmacci Q, Gabbi C, Cacchiloli A, Gonizzi G. J Mater Sci Mater Med 1994;5:345.

[5] Klein CPAT, Wolke JGC, de Blieck-Hogervorst JMA, de Groot K. J Biomed Mater Res 1994;28:909.

[6] Hing KA, Best SM, Bonfield W. J Mater Sci Mater Med 1999;10:135.

[7] Yang CY, Lin RM, Wang BC, Lee TM, Chang E, Hang YS, Chen PQ. J Biomed Mater Res 1997;37:335.

[8] Cleries L, Fernandez-Pradas JM, Morenza JL. Biomaterials 2000;21:1861.

[9] Gross KA, Berndt CC. J Biomed Mater Res 1998;39:580.

[10] Ogiso M, Yamashita Y, Matsumoto T. J Biomed Mater Res 1998;41:296.

[11] McPherson R, Gane N, Bastow TJ. J Mater Sci Mater Med 1995;6:327.

[12] Bianchi L, Leger AC, Vardelle M, Vardelle A, Fauchais P. Thin Solid Films 1997;305:35.

[13] Montavon G, Sampath S, Berndt CC, Herman H, Coddet C. J Therm Spray Technol 1995;4:67.

[14] Gougeon P, Moreau C. J Therm Spray Technol 2001;10:76.

[15] Suominen E, Aho AJ, Vedel E, Kangasniemi I, Uusipaikka E, Yli-Urpo A. J Biomed Mater Res 1996;32:543.

[16] Li H, Khor KA, Cheang P. Mater Sci Eng A 2000;293:71.

[17] Kokubo T, Kushitani H, Sakka S, Kitsugi T, Yamamuro T. J Biomed Mater Res 1990;24:721.

[18] Li H, Khor KA, Cheang P. Biomaterials 2002;23:2015.

[19] Wen J, Leng Y, Chen J, Zhang C. Biomaterials 2000;21:1339.

[20] Cuscó R, Guitián F, de Aza S, Artús L. J Europ Ceram Soc 1998;18:1301.

[21] Silva CC, Thomazini D, Pinheiro AG, Lanciotti F, Sasaki JM, Góes JC, Sombra ASB. J Phy Chem Solids 2002;63:1745.

[22] Penel G, Leroy G, Rey C, Sombret B, Huvenne JP, Bres E. J Mater Sci Mater Med 1997;8:271.

[23] Ducheyne P, Radin S, King L. J Biomed Mater Res 1993;27:25.

[24] Liao C, Lin F, Chen K, Sun J. Biomaterials 1999;20:1807.

[25] Zhou J, Zhang X, Chen J, Zeng S, de Groot K. J Mater Sci Mater Med 1993;4:83.

[26] Khor KA, Li H, Cheang P, Boey SY. Biomaterials 2003;24:723.

[27] Cleries L, Fernandez-Pradas JM, Sardin G, Morenza JL. Biomaterials 1998;19:1483.

[28] Gross KA, Berndt CC, Herman H. J Biomed Mater Res 1998;39:407.